BULLETIN OF THE POLISH ACADEMY OF SCIENCES
TECHNICAL SCIENCES, Vol. 71(6), 2023, Article number: e147062
DOI: 10.24425/bpasts.2023.147062

Experimental identification of the force and moment characteristic of symmetrically and non-symmetrically profiled annular seals

Maximilian M. G. KUHR*, and Peter F. PELZ

Chair of Fluid Systems, Technische Universität Darmstadt, Otto-Berndt-Straße 2, 64287 Darmstadt, Germany

Abstract. In modern turbomachinery, the performance and reliability is often limited by shaft vibrations induced by fluid film forces and moments of (i) plain or (ii) profiled annular seals. Therefore, these narrow annuli are mainly responsible for the overall system behaviour, i.e. safe operation and maintenance intervals. However, many studies focus only on the characteristics from the forces due to the translational motion, although the influence of the rotordynamic tilt and moment coefficients is well known. Therefore, these additional coefficients are much less researched. Especially, for profiled seals, the availability of reliable experimental data for validation purpose is rare. To overcome this fact, a test rig is operated at the Chair of Fluid Systems at the Technische Universität Darmstadt. The generic experiments presented here investigate the force and moment characteristic of plain, symmetrically profiled and non-symmetrically profiled annular seals within the relevant parameter range for turbulent flows in pumps. The investigations focus on the influence of the annulus length as well as the pressure difference across the annulus.

Key words: dynamic force and moment characteristics; annular seals; damper seals; experiments.

1. INTRODUCTION

The overall system behaviour of turbomachinery, i.e. the amplitudes at resonance and the location of the natural frequencies, is, in general, highly influenced by the dynamic characteristics of fluid-filled narrow annular gaps such as journal bearings or annular seals. In particular, the dynamic characteristics of seals, which are often manufactured with a profiled surface, such as labyrinth seals, pose a challenge for fast and reliable prediction of their dynamic properties. One reason for this is the limited availability of reliable experimental data for validation purposes, cf. Kuhr *et al.* [1]. Typically, the dynamic characteristics of narrow annuli are modelled by using classical mechanical elements, namely springs, dampers and masses, cf. Hagg [2], Hagg & Sankey [3] and Childs [4]. Accordingly, the system is characterised by using the rotordynamic coefficients: stiffness $\tilde{K}$, damping $\tilde{C}$ and inertia $\tilde{M}$. Throughout the paper, the tilde $\tilde{\square}$ characterises dimensional variables. According to Childs [5], the generalised equation of motion, including forces and moments of the annular gap flow yields

$$
-\begin{bmatrix} \tilde{F}_X \\ \tilde{F}_Y \\ \tilde{M}_X \\ \tilde{M}_Y \end{bmatrix} = \begin{bmatrix} \tilde{K} & \tilde{k} & -\tilde{K}_{\varepsilon\alpha} & \tilde{k}_{\varepsilon\alpha} \\ -\tilde{k} & \tilde{K} & -\tilde{k}_{\varepsilon\alpha} & -\tilde{K}_{\varepsilon\alpha} \\ -\tilde{K}_{\alpha\varepsilon} & \tilde{k}_{\alpha\varepsilon} & -\tilde{K}_{\alpha} & \tilde{k}_{\alpha} \\ -\tilde{k}_{\alpha\varepsilon} & -\tilde{K}_{\alpha\varepsilon} & -\tilde{k}_{\alpha} & -\tilde{K}_{\alpha} \end{bmatrix} \begin{bmatrix} \tilde{X} \\ \tilde{Y} \\ \alpha_X \\ \beta_Y \end{bmatrix}
$$
$$
+ \begin{bmatrix} \tilde{C} & \tilde{c} & \tilde{C}_{\varepsilon\alpha} & \tilde{c}_{\varepsilon\alpha} \\ -\tilde{c} & \tilde{C} & -\tilde{c}_{\varepsilon\alpha} & \tilde{C}_{\varepsilon\alpha} \\ -\tilde{C}_{\alpha\varepsilon} & \tilde{c}_{\alpha\varepsilon} & \tilde{C}_{\alpha} & \tilde{c}_{\alpha} \\ -\tilde{c}_{\alpha\varepsilon} & -\tilde{C}_{\alpha\varepsilon} & -\tilde{c}_{\alpha} & \tilde{C}_{\alpha} \end{bmatrix} \begin{bmatrix} \dot{\tilde{X}} \\ \dot{\tilde{Y}} \\ \dot{\tilde{\alpha}}_X \\ \dot{\tilde{\beta}}_Y \end{bmatrix}
$$
$$
+ \begin{bmatrix} \tilde{M} & 0 & 0 & -\tilde{m}_{\varepsilon\alpha} \\ 0 & \tilde{M} & \tilde{m}_{\varepsilon\alpha} & 0 \\ -\tilde{M}_{\alpha\varepsilon} & 0 & \tilde{M}_{\alpha} & 0 \\ 0 & -\tilde{M}_{\alpha\varepsilon} & 0 & \tilde{M}_{\alpha} \end{bmatrix} \begin{bmatrix} \ddot{\tilde{X}} \\ \ddot{\tilde{Y}} \\ \ddot{\tilde{\alpha}}_X \\ \ddot{\tilde{\beta}}_Y \end{bmatrix} . \quad (1)
$$

Here, $\tilde{F}_X, \tilde{F}_Y$ and $\tilde{M}_X, \tilde{M}_Y$ are the induced forces and moments of the seal acting on the rotor. The translational motion, velocity and acceleration of the rotor is given by $\tilde{X}, \dot{\tilde{X}}, \ddot{\tilde{X}}$ and $\tilde{Y}, \dot{\tilde{Y}}, \ddot{\tilde{Y}}$, whereas $\alpha_X, \dot{\tilde{\alpha}}_X, \ddot{\tilde{\alpha}}_X$ and $\beta_Y, \dot{\tilde{\beta}}_Y, \ddot{\tilde{\beta}}_Y$ denotes the angular motion, velocity and acceleration of the rotor around the $\tilde{X}$ and $\tilde{Y}$ axis. Equation 1 can be written in an alternative form with the definition of the individual sub-matrices based on the four different combinations: (I) induced forces on the rotor from translational motion, (II) induced forces on the rotor from angular motion, (III) induced moments on the rotor from translational motion and (IV) induced moments on the rotor from angular motion

*e-mail: maximilian.kuhr@tu-darmstadt.de

Manuscript submitted 2023-05-02, revised 2023-05-02, initially accepted for publication 2023-08-14, published in December 2023.

© 2023 The Author(s). This is an open access article under the CC BY license (http://creativecommons.org/licenses/by/4.0/)

$$-\begin{bmatrix}\tilde{F}_X\\ \tilde{F}_Y\\ \tilde{M}_X\\ \tilde{M}_Y\end{bmatrix}=\begin{bmatrix}\tilde{\boldsymbol{K}}_{\mathrm{I}} & \tilde{\boldsymbol{K}}_{\mathrm{II}}\\ \tilde{\boldsymbol{K}}_{\mathrm{III}} & \tilde{\boldsymbol{K}}_{\mathrm{IV}}\end{bmatrix}\begin{bmatrix}\tilde{X}\\ \tilde{Y}\\ \alpha_X\\ \beta_Y\end{bmatrix}+\begin{bmatrix}\tilde{\boldsymbol{C}}_{\mathrm{I}} & \tilde{\boldsymbol{C}}_{\mathrm{II}}\\ \tilde{\boldsymbol{C}}_{\mathrm{III}} & \tilde{\boldsymbol{C}}_{\mathrm{IV}}\end{bmatrix}\begin{bmatrix}\dot{\tilde{X}}\\ \dot{\tilde{Y}}\\ \dot{\tilde{\alpha}}_X\\ \dot{\tilde{\beta}}_Y\end{bmatrix}+\begin{bmatrix}\tilde{\boldsymbol{M}}_{\mathrm{I}} & \tilde{\boldsymbol{M}}_{\mathrm{II}}\\ \tilde{\boldsymbol{M}}_{\mathrm{III}} & \tilde{\boldsymbol{M}}_{\mathrm{IV}}\end{bmatrix}\begin{bmatrix}\ddot{\tilde{X}}\\ \ddot{\tilde{Y}}\\ \ddot{\tilde{\alpha}}_X\\ \ddot{\tilde{\beta}}_Y\end{bmatrix}. \tag{2}$$

The geometries of the sealing gaps are manifold and depend on different boundary conditions. In accordance with the requirements, plain or profiled seals, cf. Fig. 1, are used. Typically, the rotordynamic coefficients depend on three different characteristics of the annulus: (i) the geometry of the annular gap, i.e. the gap length $\tilde{L}$, the shaft radius $\tilde{R}$, the mean gap clearance $\bar{\tilde{h}}$ and the gap function $\tilde{h}=\tilde{h}(\varphi,\tilde{z},\tilde{t})$ with the circumferential and axial coordinate $\varphi,\tilde{z}$ and the surface profiling; (ii) the operating conditions, i.e. the eccentric and angular position of the shaft $\tilde{e},\alpha_X,\beta_Y$, the distance of the centre of rotation $\tilde{z}_T$ from the annulus entrance, the mean axial velocity $\bar{\tilde{C}}_z$, the angular velocity of the shaft $\tilde{\Omega}$ and the pre-swirl velocity at the annulus inlet $\tilde{C}_\varphi|_{z=0}$; (iii) the lubricant characteristics, i.e. the dynamic viscosity $\tilde{\eta}$ and the fluid density $\tilde{\rho}$. On dimensional ground, cf. Kuhr [7–9], the dimensionless rotordynamic coefficients are only a function of 8 dimensionless measures and the surface profiling: (i) the dimensionless annulus length $L:=\tilde{L}/\tilde{R}$, (ii) the relative eccentricity $\varepsilon:=\tilde{e}/\bar{\tilde{h}}$, (iii, iv + v) the normalised angular displacements $\alpha:=\tilde{L}\,\alpha_X/\bar{\tilde{h}}$ and $\beta:=\tilde{L}\,\beta_Y/\bar{\tilde{h}}$ around the dimensionless fulcrum $z_T:=\tilde{z}_T/\tilde{L}$, (vi) the modified Reynolds number in circumferential direction $\psi Re^*_\varphi:=(\bar{\tilde{h}}/\tilde{R})\,(\tilde{\Omega}\tilde{R}\bar{\tilde{h}}/\tilde{\nu})^{n_\mathrm{f}}$, (vii) the flow number $\phi:=\bar{\tilde{C}}_z/(\tilde{\Omega}\tilde{R})$, (viii) the dimensionless pre-swirl $C_\varphi|_{z=0}:=\tilde{C}_\varphi|_{z=0}/(\tilde{\Omega}\tilde{R})$. Here, $\psi:=\bar{\tilde{h}}/\tilde{R}$ is the gap clearance and n_f is an empirical constant describing an arbitrary line within the double logarithmic Moody diagram, cf. Lang [6] and Kuhr *et al.* [8, 10]

$$K_{ij},C_{ij},M_{ij}=\mathrm{f}\left(L,\varepsilon,\alpha,\beta,z_T,Re^*_\varphi,\phi,C_\varphi|_{z=0},\mathrm{PROFILING}\right). \tag{3}$$

The dimensionless rotordynamic coefficients are separately defined for the forces and moments acting on the rotor due to translational and angular motions

$$\begin{aligned}K_{\mathrm{I}}&:=\frac{2\bar{\tilde{h}}\tilde{K}_{ij}}{\tilde{\rho}\tilde{\Omega}^2\tilde{R}^3\tilde{L}}, & K_{\mathrm{II}}&:=\frac{2\bar{\tilde{h}}\tilde{K}_{\mathrm{II}}}{\tilde{\rho}\tilde{\Omega}^2\tilde{R}^3\tilde{L}^2},\\ K_{\mathrm{III}}&:=\frac{2\bar{\tilde{h}}\tilde{K}_{\mathrm{III}}}{\tilde{\rho}\tilde{\Omega}^2\tilde{R}^3\tilde{L}^2}, & K_{\mathrm{IV}}&:=\frac{2\bar{\tilde{h}}\tilde{K}_{\mathrm{IV}}}{\tilde{\rho}\tilde{\Omega}^2\tilde{R}^3\tilde{L}^3}.\end{aligned} \tag{4}$$

Here, the first two stiffness coefficients represent dynamic force coefficients due to translational and angular motion, whereas the later ones represent the moment coefficients. The indices represent the corresponding sub-matrices of equation 1. The damping and inertia terms are defined accordingly

$$\begin{aligned}C_I&:=\frac{2\bar{\tilde{h}}\tilde{C}_I}{\tilde{\rho}\tilde{\Omega}\tilde{R}^3\tilde{L}}, & C_{II}&:=\frac{2\bar{\tilde{h}}\tilde{C}_{II}}{\tilde{\rho}\tilde{\Omega}\tilde{R}^3\tilde{L}^2},\\ C_{III}&:=\frac{2\bar{\tilde{h}}\tilde{C}_{III}}{\tilde{\rho}\tilde{\Omega}\tilde{R}^3\tilde{L}^2}, & C_{IV}&:=\frac{2\bar{\tilde{h}}\tilde{C}_{IV}}{\tilde{\rho}\tilde{\Omega}\tilde{R}^3\tilde{L}^3},\end{aligned} \tag{5a}$$

$$\begin{aligned}M_I&:=\frac{2\bar{\tilde{h}}\tilde{M}_I}{\tilde{\rho}\tilde{R}^3\tilde{L}}, & M_{II}&:=\frac{2\bar{\tilde{h}}\tilde{M}_{II}}{\tilde{\rho}\tilde{R}^3\tilde{L}^2},\\ M_{III}&:=\frac{2\bar{\tilde{h}}\tilde{M}_{III}}{\tilde{\rho}\tilde{R}^3\tilde{L}^2}, & M_{IV}&:=\frac{2\bar{\tilde{h}}\tilde{M}_{IV}}{\tilde{\rho}\tilde{R}^3\tilde{L}^3}.\end{aligned} \tag{5b}$$

Although at some point, especially for long seals, all 48 rotordynamic coefficients have to be considered during the design process of modern turbomachinery, cf. Childs [11] and Kuhr *et al.* [8], most of the experimental and analytical studies only focus on the dynamic characteristics resulting from the forces on the rotor due to its translational motion. Therefore, the additional rotordynamic tilt and moment coefficients, especially for the use of profiled seal geometries, are much less researched. Furthermore, even if there is a variety of models capable of predicting not only the dynamic forces but also the moments on the rotor, cf. Childs [5], Simon & Frêne [12, 13], San Andrés [14–16], Storteig [17], Gibbons *et al.* [18], Gibbons & Goyne [19], it is difficult to validate the prediction quality of the developed methods due to the non-availability of

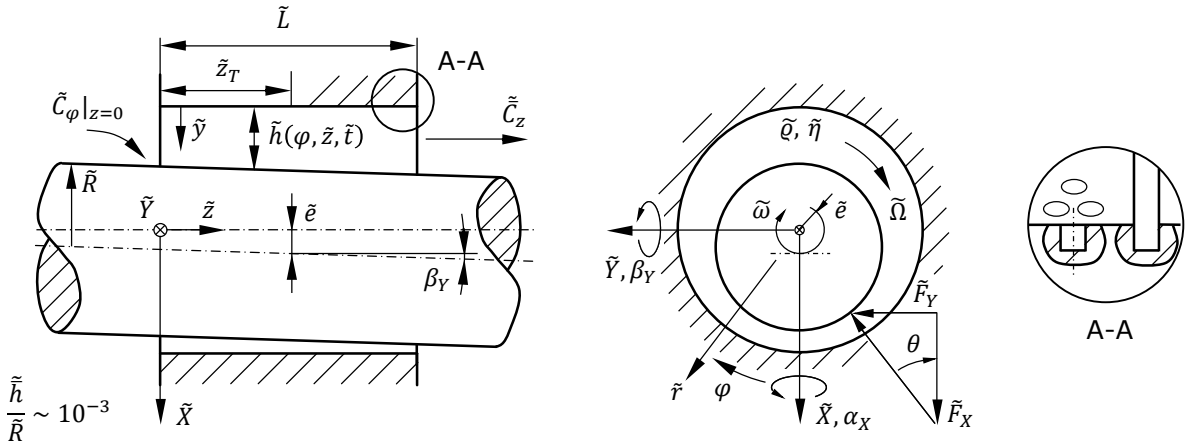

Fig. 1. Generic annular seal geometry, cf. Lang [6], Kuhr [7] and Kuhr *et al.* [8]

experimental validation data, especially for profiled seals. For plain annular seals, however, there are a few publications experimentally identifying also the tilt and moment coefficients. One of the first publications including the experimental investigation including the tilt and moment coefficients is the infamous work of Kanemori & Iwatsubo [20, 21]. Thanks to a specially constructed test rig, consisting of two rotors mounted and driven in each other, small translational as well as rotational movements around the static rest position induce frequency-dependent forces and moments on the rotor. Kanemori & Iwatsubo, essentially, investigate the influence of the axial pressure difference as well as the influence of the angular frequency of the rotor and the influence of the pre-swirl. In parallel, Neumer [22] and Matros et al. [23] use active magnetic bearings to position and excite the rotor. Here, mainly the influence of the angular frequency of the rotor and the influence of the axial pressure difference on the rotordynamic coefficients is investigated. To date, these papers represent the most widely used experimental validation basis. However, as stated before, none of them investigated the influence of typical surface profiles like boreholes or saw-tooth patterns on the dynamic tilt and moment characteristics. To overcome this fact, a test rig is operated at the Chair of Fluid Systems at the Technische Universität Darmstadt and briefly described in the following section. The generic experiments presented later on then investigate the force and moment characteristics not only of plain, but also of symmetrically profiled and non-symmetrically profiled annular seals.

2. ANNULAR SEAL AND BEARING TEST RIG

The experimental identification of the dynamic characteristics is carried out by using the annular seal and bearing test rig operated at the chair of fluid systems at the Technische Universität Darmstadt, cf. Kuhr [7, 9] and Kuhr *et al.* [10]. As illustrated in Fig. 2, the main components of the test rig are the gap module as well as the two active magnetic bearings (AMB) to support and excite the rotor. Compared to conventional bearings such as ball or journal bearings used by several authors, cf. Childs [11, 24], Kanemori & Iwatsubo [20, 21] and Moreland *et al.* [25], magnetic bearings have the advantage of bearing the rotor completely contactless and thus frictionless. In addition, the AMBs are an inherent force and displacement measuring system, making them ideal for identifying the dynamic characteristics of rotating machinery and components like annular seals and journal bearings. The test rig is capable of measuring both concentric and off-centred, i.e. eccentric, as well as misaligned rotor positions in an eccentricity and misalignment range of $\varepsilon = 0..0.9, \alpha_x, \beta_y = 0.15°$. By using a ten-stage centrifugal pump to supply the test rig, the axial pressure difference across the annuls $\Delta\tilde{p}$ can be varied continuously in the range of $\Delta\tilde{p} = 0..20\,\mathrm{bar}$, whereas the pre-swirl at the seal entrance can be controlled in the range of $C_\varphi\big|_{z=0} = 0..1.4$. For further information on the capabilities, calibration and uncertainty of the test rig, please refer to the work of Kuhr [7, 9] and Kuhr *et al.* [10].

2.1. Identification procedure

Since the rotordynamic force and moment characteristics cannot be measured directly, they must be determined by using parameter identification methods, i.e. linear and quadratic regressions. Kuhr [7, 9] extended the formerly presented test rig to include excitation of the shaft in the four degrees of freedom $\tilde{X}, \tilde{Y}$ and α_X, β_Y. To do so, four linear independent user-defined whirling motions at different whirling frequencies with and against the rotation of the rotor are used and the induced dynamic forces and torques on the rotor are measured using the active magnetic bearings. Based on the work of Childs &

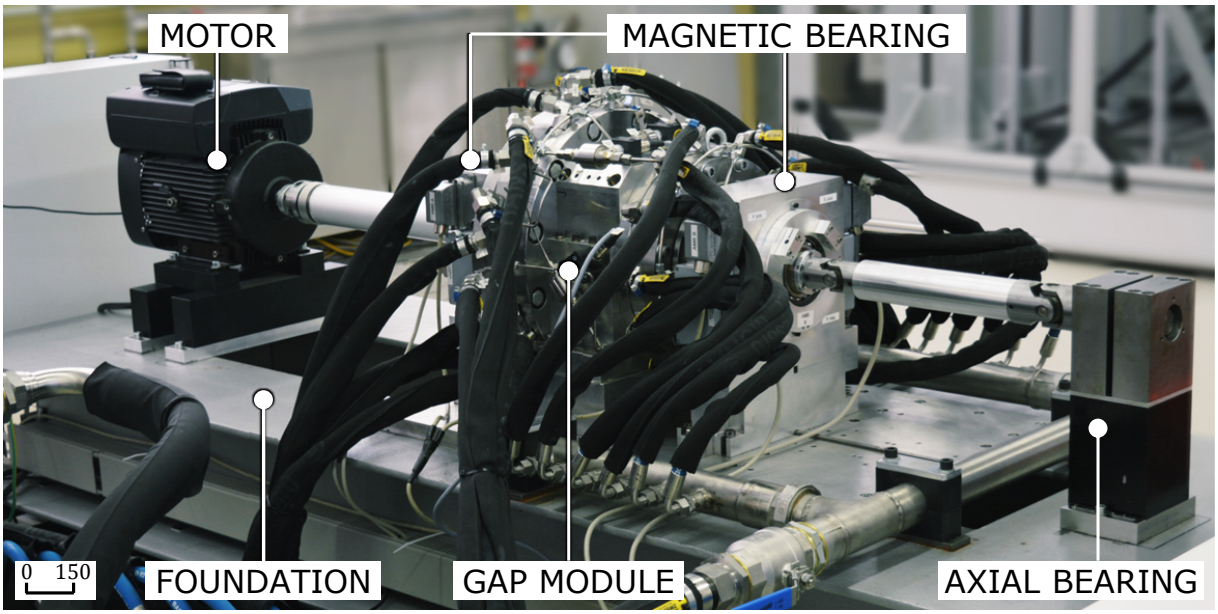

Fig. 2. The annular seal and bearing test rig at the Chair of Fluid Systems at the Technische Universität Darmstadt, cf. Kuhr [7, 9] and Kuhr *et al.* [10]

Hale [24], the equation of motion 1 is transformed into the frequency domain to identify the rotordynamic coefficients using linear and quadratic regression techniques. The complex equation of motion in the frequency domain yields

$$-\begin{bmatrix}\tilde{\mathcal{F}}_X\\ \tilde{\mathcal{F}}_Y\\ \tilde{\mathcal{M}}_X\\ \tilde{\mathcal{M}}_Y\end{bmatrix}=\begin{bmatrix}\tilde{\mathcal{K}}_{XX} & \tilde{\mathcal{K}}_{XY} & \tilde{\mathcal{K}}_{X\alpha} & \tilde{\mathcal{K}}_{X\beta}\\ \tilde{\mathcal{K}}_{XY} & \tilde{\mathcal{K}}_{YY} & \tilde{\mathcal{K}}_{Y\alpha} & \tilde{\mathcal{K}}_{Y\beta}\\ \tilde{\mathcal{K}}_{\alpha X} & \tilde{\mathcal{K}}_{\alpha Y} & \tilde{\mathcal{K}}_{\alpha\alpha} & \tilde{\mathcal{K}}_{\alpha\beta}\\ \tilde{\mathcal{K}}_{\beta X} & \tilde{\mathcal{K}}_{\beta Y} & \tilde{\mathcal{K}}_{\beta\alpha} & \tilde{\mathcal{K}}_{\beta\beta}\end{bmatrix}\begin{bmatrix}\tilde{\mathcal{D}}_X\\ \tilde{\mathcal{D}}_Y\\ \mathcal{D}_{\alpha_X}\\ \mathcal{D}_{\beta_Y}\end{bmatrix}.$$

Here, $\tilde{\mathcal{K}}_{ij}$ are the complex stiffness coefficients depending on the user-defined whirling frequency $\tilde{\omega}$. $\tilde{\mathcal{F}}=\mathfrak{F}(\tilde{F})$ and $\tilde{\mathcal{M}}=\mathfrak{F}(\tilde{M})$ are the Fourier transformations of the induces forces and moments, whereas $\tilde{\mathcal{D}}_i=\mathfrak{F}(\tilde{\imath})$ are the Fourier transforms of the translational and angular excitation amplitudes. The real part of the complex stiffness coefficients $\Re\left(\tilde{\mathcal{K}}_{ij}\right)$ contains the stiffness and inertia coefficient, whereas the imaginary part $\Im\left(\tilde{\mathcal{K}}_{ij}\right)$ contains the damping coefficients

$$\begin{aligned}\tilde{\mathcal{K}}_{ij}&=\tilde{K}_{ij}-\tilde{M}_{ij}\,\tilde{\omega}^2+\mathrm{i}\tilde{C}_{ij}\,\tilde{\omega},\quad\text{with}\\ \Re\left(\tilde{\mathcal{K}}_{ij}\right)&=\tilde{K}_{ij}-\tilde{M}_{ij}\,\tilde{\omega}^2,\quad\text{and}\quad\Im\left(\tilde{\mathcal{K}}_{ij}\right)=\tilde{C}_{ij}\,\tilde{\omega}.\end{aligned}\tag{6}$$

By examining equation 6, it becomes clear, that the rotordynamic coefficients can be determined by a linear or quadratic least mean square fit if the system is excited with at least two independent user-defined whirling frequencies. To improve the accuracy of the regression, at least five whirling frequencies were used during the experiments. With the independent motions necessary for identification, this results in a number of 20 individual measurements for the identification of all rotordynamic coefficients. For further information on the identification procedure and its uncertainty, please refer to the work of Kuhr [7, 9].

3. RESULTS AND DISCUSSION

3.1. Seal geometries and steady-state operating conditions

The experimental investigations are carried out using three different seal geometries at four and two lengths respectively. Figure 3 shows the three investigated geometries. The seal geometries are chosen to represent typical geometries in modern turbomachinery. In addition to plain, non-profiled seals, two surface-profiled annuli are investigated: (i) seals with symmetrical profiles, i.e. sawtooth patterns, and (ii) non-symmetrical profiles, i.e. borehole-profiled annuli. The dimensionless lengths of the seals investigated are $L=0.216$, 0.4, 0.6 and 1.6 for the plain and non-symmetrically profiled ones, whereas the symmetrically profiled seals are only investigated for $L=0.6$ and 1.6. All experiments are conducted using water at a temperature of 35°C with a concentric, non-tilted rotor inside the annulus, i.e. $\varepsilon=\alpha_X=\beta_Y=0$. The centre of rotation is placed in the middle of each annulus, i.e. $z_T=0.5$ and the pre-swirl at the seal entrance $C_\varphi|_{z=0}$ as well as the modified Reynolds number Re^*_φ are kept constant at $C_\varphi|_{z=0}=0.5$

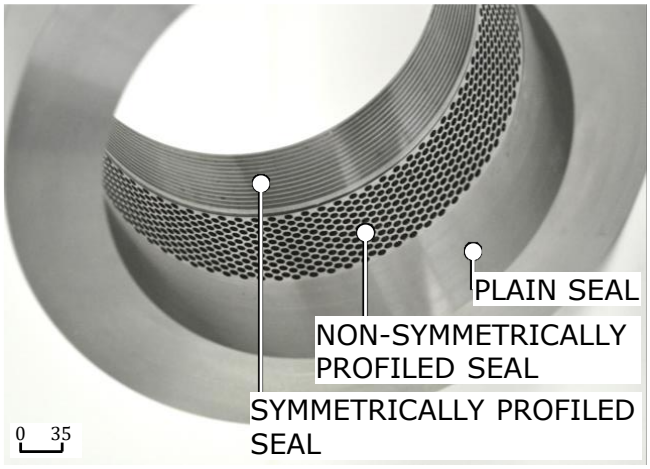

Fig. 3. Physical image of the plain, symmetrically profiled and non-symmetrically profiled seal

and $Re^*_\varphi=0.017$. Here, the chosen modified Reynolds number corresponds to a relative seal clearance of $\psi=2.6‰$ and a Reynolds number of $Re_\varphi=2800$, indicating fully turbulent flow inside the annulus. For the investigations regarding the influence of the seal length, the dimensionless axial pressure difference $\Delta p:=2\Delta\tilde{p}/(\tilde{\rho}\tilde{\Omega}^2\tilde{R}^2)$ is kept constant $\Delta p=\text{const}=9.0$, whereas for the experiments dealing with the influence of Δp, the pressure difference is varied on a range of $\Delta p=4.8..16$ at a constant seal length $L=1.6$.

3.2. Leakage characteristic

Before discussing the dynamic force and moment characteristics of the seals, the influence of the length L and the pressure difference Δp on the leakage, i.e. the flow number ϕ

$$\phi:=\tilde{\bar{C}}_z/(\tilde{\Omega}\tilde{R}),\tag{7}$$

is initially investigated. Figure 4 shows the influence of the seal length L (left) and the axial pressure difference Δp (right) on the flow number ϕ. Within the picture, the circles represent the measurement results of the plain seals, whereas the triangles and diamonds represent the results for the symmetrically and non-symmetrically profiled geometries. First, examining the effects of surface profiling at different seal lengths, a significant reduction of the seal leakage, i.e. the flow number, is observed when comparing the plain and profiled annuli. Here, the non-symmetrically profiled seal has the lowest leakage, followed by the non-symmetrically and the plain annular seal. As the gap length increases, the leakage of all three geometries decreases due to the increased friction within the annulus. Remarkably, the difference between the symmetrically and non-symmetrically profiled seals becomes smaller with increasing length. Second, the influence of the axial pressure difference is investigated. It exhibits that all three geometries show the typical proportionality to the axial pressure difference, i.e $\phi\sim\Delta p^{0.50}$. However, the non-symmetrically profiled seal shows a better leakage characteristic, i.e. flow number ϕ, at lower axial pressure differences compared to the symmetrically profiled one.

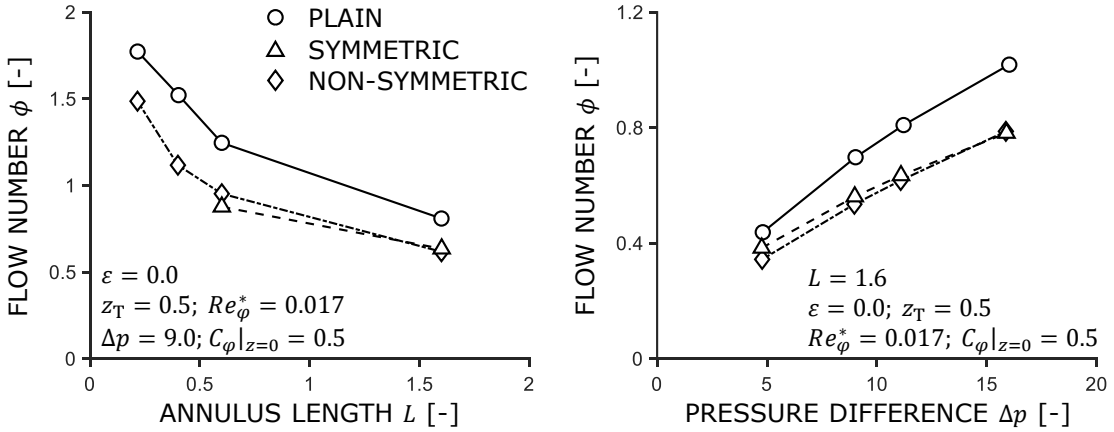

Fig. 4. Influence of the annulus length L (left) and pressure difference Δp (right) on the leakage characteristic, i.e. the flow number ϕ, of the plain, symmetric and non-symmetric profiled annulus

3.3. Influence of the annulus length on the dynamic characteristics

Subsequently, to the investigations regarding the static leakage characteristic, the dynamic force and moment characteristics of the plain and profiled seals are examined. Figures 5 to 7 show the dimensionless stiffness $\boldsymbol{K}$, damping $\boldsymbol{C}$ and inertia $\boldsymbol{M}$ coefficients. The individual diagrams in the figures are arranged according to the sub-matrices I to IV, cf. equation 1, beginning with the first sub-matrix I, i.e. the coefficients from the forces due to translational motion. The left-hand side of each figure shows the direct coefficients, whereas the cross-coupled coefficients are located on the right-hand side. The definition of the different markers for plain, symmetrically and non-symmetrically profiled seals remains unchanged. It should be noted that for the sub-matrices II to IV only lengths $L \geq 0.4$ are displayed. This is because of the shortest length investigated, $L = 0.216$, the angular motion of the rotor could not be measured properly.

Stiffness coefficients

Figure 5 shows the results for the stiffness coefficients $\boldsymbol{K}$ when varying the seal length L, as well as the influence of the surface profiles. First, the results for the sub-matrices I and II, i.e. the stiffness coefficients K, k and $K_{\varepsilon\alpha}, k_{\varepsilon\alpha}$, are examined. It exhibits that the direct and cross-coupled stiffness K and $k_{\varepsilon\alpha}$ decrease with increasing seal length, whereas the cross-coupled stiffness k increases and the direct stiffness $K_{\varepsilon\alpha}$ is independent of the annular seal length. The results, namely the decrease in direct and cross-coupled stiffness K and $k_{\varepsilon\alpha}$ seem contradictory at first. However, the decrease in stiffness results from the chosen dimensionless form of the coefficients, cf. equations 4 and 5. Here, the rotordynamic coefficients are made dimensionless by using the seal length L. This can result in a decreasing value for the dimensionless stiffness coefficients, even if the dimensional stiffness coefficients $\tilde{K}$ increase with the seal length. Regarding the effect of symmetrical and non-symmetrical surface profiles, it exhibits that the profiling mostly affects the direct and cross-coupled stiffness K and $k_{\varepsilon\alpha}$. Here, the symmetrically profiled seals exhibit the lowest stiffness values, followed by the non-symmetrical ones and the plain annulus. The cross-coupled stiffness k and the direct stiffness $K_{\varepsilon\alpha}$ appear to be uninfluenced by the profiling except at the largest seal length $L = 1.6$. Here, the cross-coupled stiffness k of the symmetrically profiled seal is approximately half of the one from the plain and non-symmetrically profiled seal. It should be noted that even for small lengths, the coefficients from the second sub-matrix II, i.e. the tilt coefficients $K_{\varepsilon\alpha}, k_{\varepsilon\alpha}$ are in the same order of magnitude as the stiffness coefficients on sub-matrix I. Second, the results for the sub-matrices III and IV, i.e. the stiffness coefficients $K_{\alpha\varepsilon}, k_{\alpha\varepsilon}$ and K_α, k_α, are examined. Here, all stiffness coefficients exhibit a decreasing value with the seal length being increased. In contrast, of the coefficients of sub-matrix I and II, the influence of the surface profiling is only visible within the direct stiffness K_α of sub-matrix IV. Here, the non-symmetrically profiled seal exhibits the highest stiffness values, followed by the symmetrically and plain seal geometry. It should be noted that the high stiffness values of the direct coefficient K_α have to be interpreted with caution. Due to the small length of the seal, e.g. $L = 0.4$, the dimensional induced forces and moments $\tilde{F}$ and $\tilde{M}$ are small compared to the ones at seal with length $L = 1.6$. This can lead to high uncertainty in the identified rotordynamic coefficients, especially the additional tilt and moment ones.

Damping coefficients

Figure 6 shows the results for the damping coefficients $\boldsymbol{C}$ when varying the seal length L. Following the explanations of the stiffness coefficients, the results for the first and second sub-matrix I and II, i.e. the damping coefficients C, c and $C_{\varepsilon\alpha}, c_{\varepsilon\alpha}$, are examined first. In contrast to the stiffness coefficients, the damping coefficients increase with increasing seal length. However, similar to the stiffness coefficients, the influence of the surface profiling is mainly visible in the direct and cross-coupled damping coefficients C and $c_{\varepsilon\alpha}$. Here, the non-symmetrically profiled seal exhibits the highest damping values, followed by the plain and the symmetrically profiled seal. It should be noted

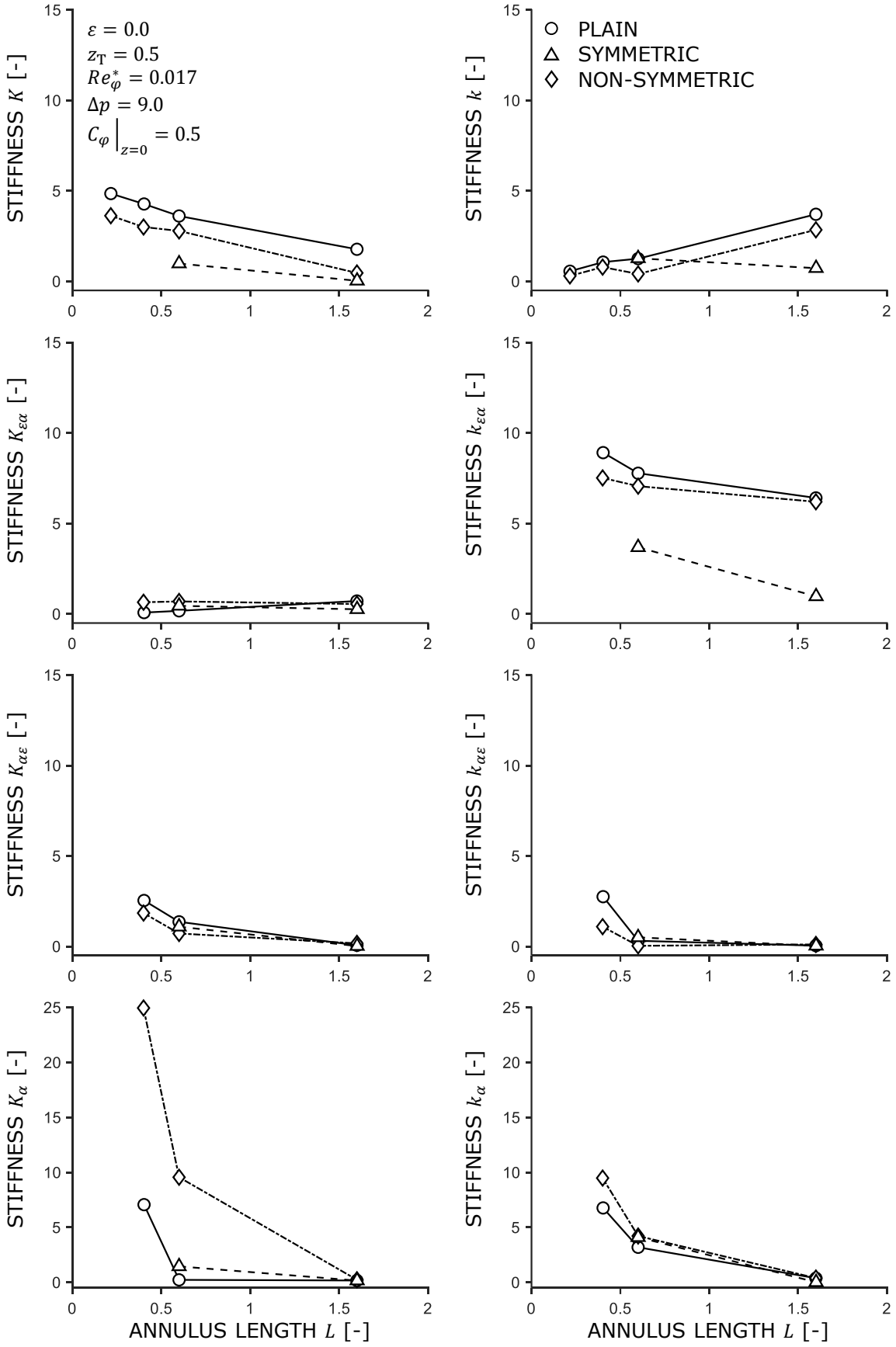

Fig. 5. Influence of the annulus length L on the stiffness coefficients $\boldsymbol{K}$ of the plain, symmetric and non-symmetric profiled seal

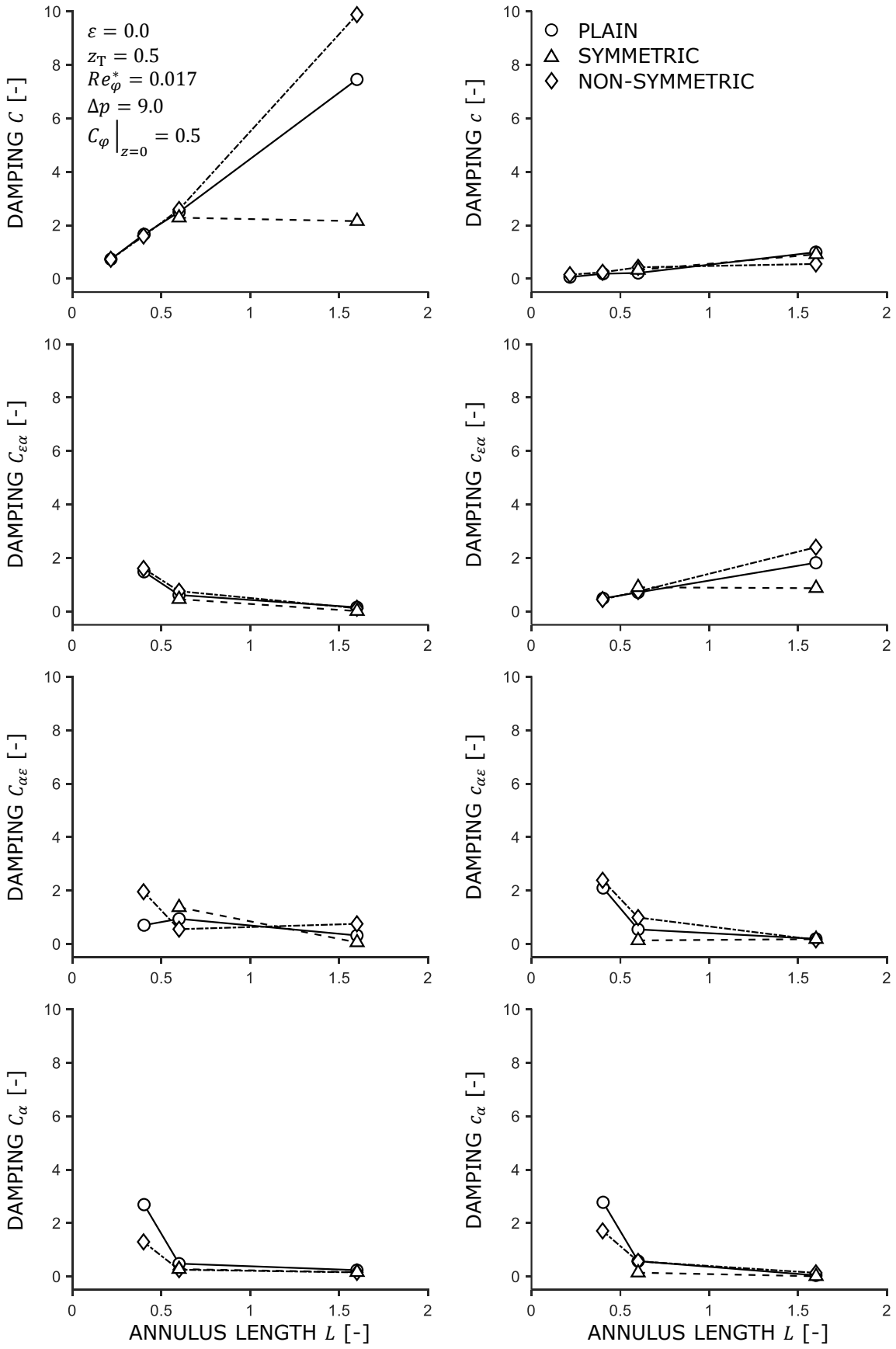

Fig. 6. Influence of the annulus length L on the damping coefficients $\boldsymbol{C}$ of the plain, symmetric and non-symmetric profiled seal

that, in contrast to the stiffness coefficients, the shortest seals actually have the smallest dimensional damping values. Focusing now on the damping coefficients of the sub-matrices III and IV, it becomes obvious that the whole damping of the seal is dominated by the direct damping coefficients of sub-matrix I, i.e. C. Although both the change in the annulus length and the profiling of the surfaces are clearly visible in the damping coefficients of sub-matrix I and II, neither the length nor the profiling has a major influence on the damping coefficients of the sub-matrices III and IV. Only at short lengths, the coefficients show a slight influence of the surface profiling.

Inertia coefficients

Finally, Fig. 7 shows the results for the inertia coefficients $\boldsymbol{M}$ when varying the seal length L. In contrast to the stiffness and damping coefficients, only the non-zero inertia coefficients, cf. equation 1, are shown. It exhibits that the direct inertia coefficients of sub-matrix I M are increasing with increasing seal length, whereas the remaining coefficients of sub-matrix II to IV, i.e. $m_{\varepsilon\alpha}$, $M_{\alpha\varepsilon}$ and M_{α}, are decreasing. Furthermore, only the direct inertia coefficients of sub-matrix I M exhibit a linear behaviour, whereas the remaining ones decrease non-linearly. Regarding the influence of the symmetrical and non-symmetrical surface profiling, it is shown that mainly the direct inertia coefficients of sub-matrix III, i.e. $M_{\alpha\varepsilon}$, exhibit a significant impact on the profiling. Here, the symmetrically profiled seal has the highest values and is followed by the plain and the non-symmetrically profiled geometry. Regarding the remaining coefficient of sub-matrix I, II and IV, the effect of the surface profiling is visible, but less pronounced.

3.4. Influence of the axial pressure difference on the dynamic characteristics

Subsequently, the investigations regarding the influence of the seal length L, the influence of the axial pressure difference Δp on the dynamic force and moment characteristics of the plain and profiled seals are examined, cf. Figs. 5 to 7. In contrast to the results shown so far, only the coefficients that experience the most significant changes due to the variation of the pressure difference Δp are shown.

Stiffness coefficients

Figure 8 shows the results for the stiffness coefficients $\boldsymbol{K}$ when varying the axial pressure difference Δp. It exhibits that mainly the direct and cross-coupled coefficients of the first and second sub-matrix I and II, i.e. K, k and $K_{\varepsilon\alpha}$, $k_{\varepsilon\alpha}$ are affected by the variation of Δp. Furthermore, the stiffness coefficients indicate a linear dependence on the axial pressure difference. Regarding the influence of the symmetrical and non-symmetrical surface profiling, the difference between the geometries increases with increasing Δp. Similar to the results concerning the influence of the seal length, the plain seal geometry exhibits the highest stiffness values followed by the non-symmetrically profiled and the symmetrically profiled one. It should be noted that the symmetrically profiled seal has negative direct stiffness values for high axial pressure differences $\Delta p > 10$.

Damping coefficients

Subsequently, for the stiffness coefficients, Fig. 9 shows the influence of the axial pressure difference Δp on the direct and cross-coupled damping coefficients of sub-matrix I and II, i.e.

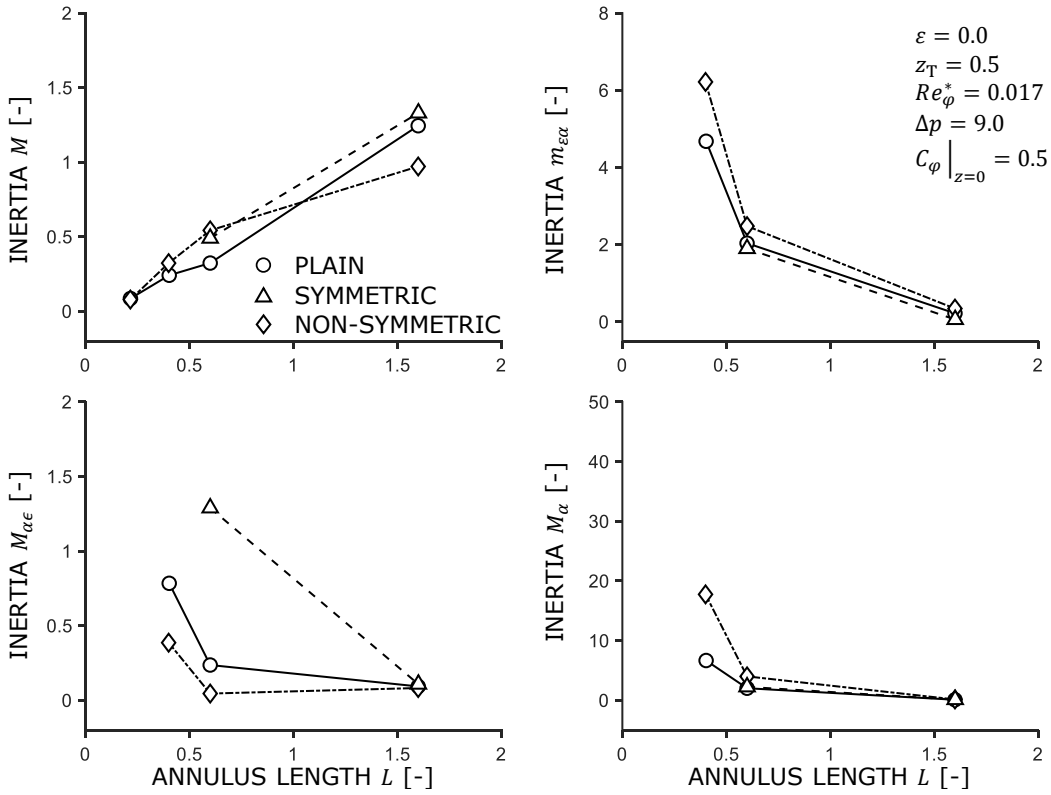

Fig. 7. Influence of the annulus length L on the inertia coefficients $\boldsymbol{M}$ of the plain, symmetric and non-symmetric profiled seal

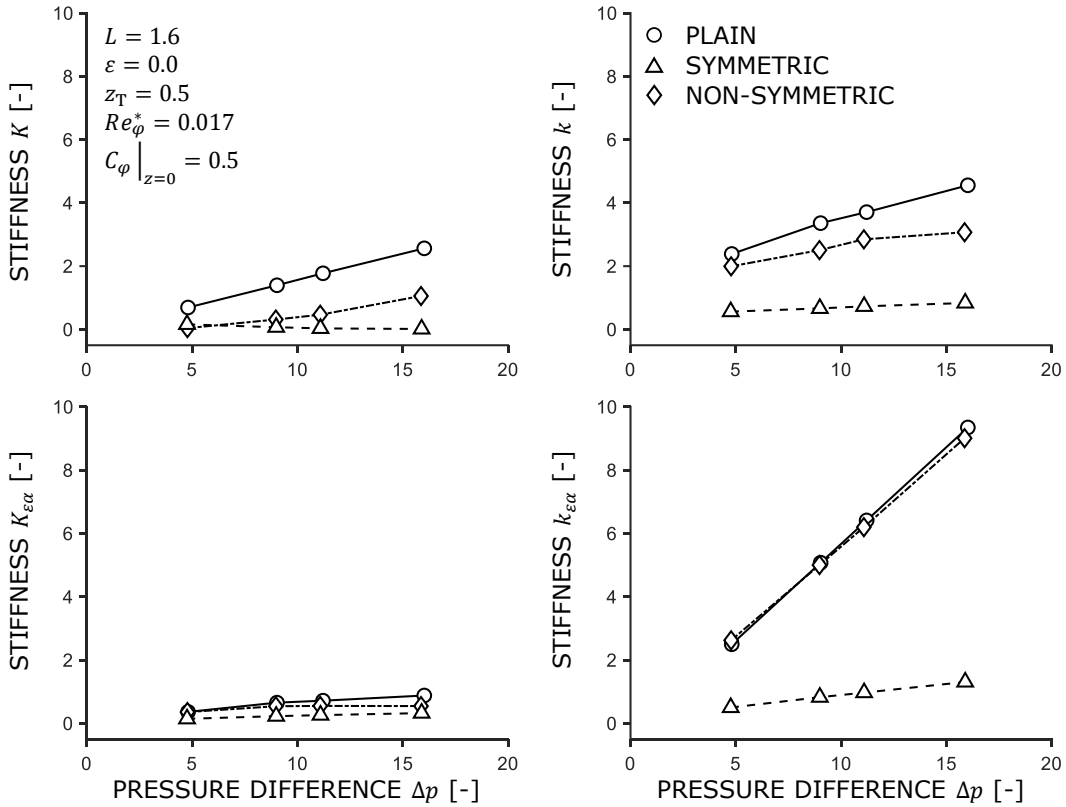

Fig. 8. Influence of the pressure difference Δp on the stiffness coefficients $\boldsymbol{K}$ of the plain, symmetric and non-symmetric profiled seal

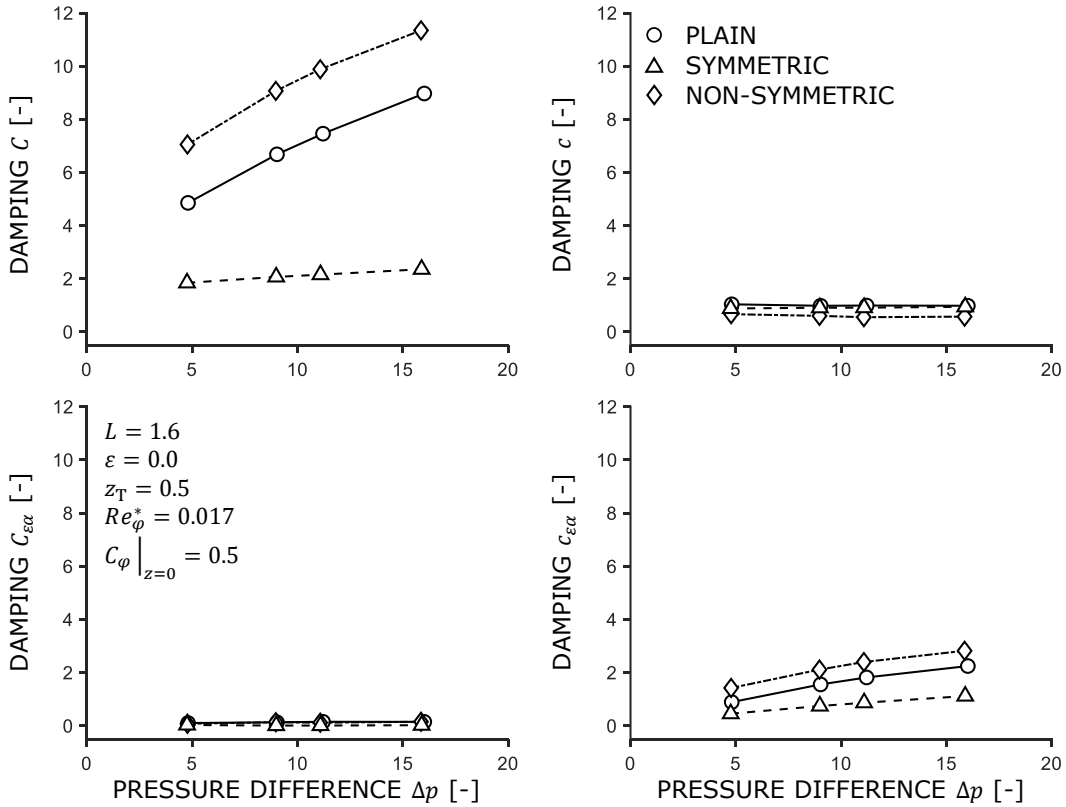

Fig. 9. Influence of the pressure difference Δp on the damping coefficients $\boldsymbol{C}$ of the plain, symmetric and non-symmetric profiled seal

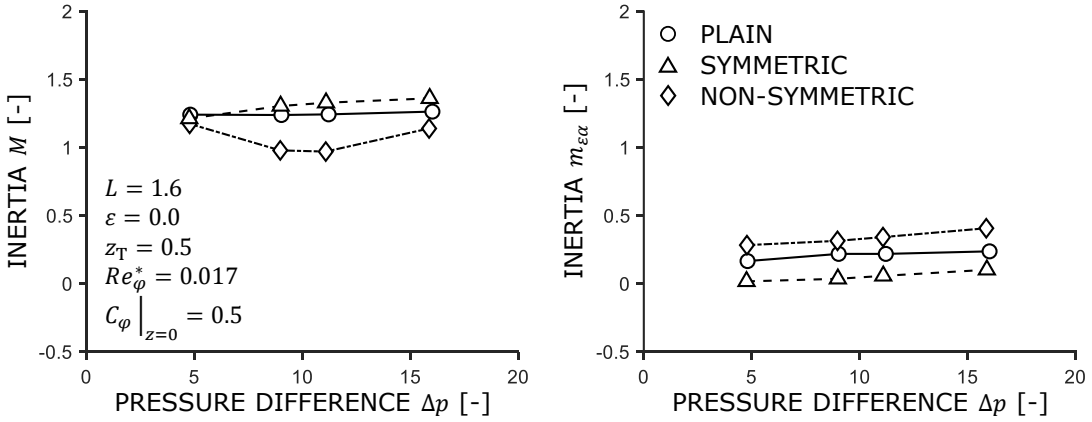

Fig. 10. Influence of the pressure difference Δp on the inertia coefficients $\boldsymbol{M}$ of the plain, symmetric and non-symmetric profiled seal

C, c and $C_{\varepsilon\alpha}$, $c_{\varepsilon\alpha}$. It is shown that mainly the direct damping C as well as the cross-coupled damping $c_{\varepsilon\alpha}$ is affected by both the axial pressure difference Δp and the surface profiling with symmetrical and non-symmetrical patterns. The effect of the surface profiling, i.e. the order of the highest damping values ranging from non-symmetrically profiled to plain and symmetrically profiled geometries, remains untouched. In contrast to the damping coefficients C and $c_{\varepsilon\alpha}$, the cross-coupled and direct damping coefficients c and $C_{\varepsilon\alpha}$ are independent of the axial pressure difference.

Inertia coefficients

Finally, the influence of the axial pressure difference on the inertia coefficients is shown in Fig. 10. Here, only the direct inertia coefficients of the first sub-matrix M and the cross-coupled inertia coefficients of the second sub-matrix $m_{\varepsilon\alpha}$ are shown. It exhibits that both the direct and cross-coupled inertia M and $m_{\varepsilon\alpha}$ are almost independent of the axial pressure difference. This is in good agreement with the latest findings of Kuhr [7], indicating that the inertia coefficients mainly depend on the geometrical parameters of the seal. However, the influence of the symmetrical and non-symmetrical surface profiling is visible in both coefficient. Here, the symmetrically profiled seal exhibits the highest values for the direct inertia M, followed by the plain and non-symmetrically profiled seal. Regarding the cross-coupled inertia coefficients $m_{\varepsilon\alpha}$, the order reverses, leading to the highest values in the non-symmetrically profiled seal.

4. CONCLUSION

In summary, the following statements can be made:

- A significant reduction of the seal leakage, i.e. the flow number ϕ, is observed when comparing the plain and profiled seal geometries. As the gap length increases, the leakage decreases due to the increased friction within the annulus. However, the difference between the symmetrically and asymmetrically profiled gaps becomes smaller with increasing seal length.
- The symmetrically profiled seal geometry is superior to the non-symmetrically profiled one and the plain seal geometry in terms of leakage.
- The use of surface profiled annular seals such as borehole and saw-tooth pattern leads to a significant change not only in the dynamic force characteristic but also in the additional tilt and moment characteristic.
- The use of non-symmetrically profiled seals leads to a reduction of the stiffness coefficients of sub-matrix I to III, i.e. K, k, $K_{\varepsilon\alpha}$, $k_{\varepsilon\alpha}$, $K_{\alpha\varepsilon}$, $k_{\alpha\varepsilon}$, whereas the stiffness coefficients of sub-matrix IV K_α, k_α are increased. Regarding the damping coefficients, the use of non-symmetrically profiled seals increases the direct damping coefficients of the first sub-matrix, i.e. C, which are the dominant coefficients for the whole damping matrix $\boldsymbol{C}$.
- The use of symmetrically profiled seals leads to a further reduction of the stiffness coefficients of sub-matrix I to III, i.e. K, k, $K_{\varepsilon\alpha}$, $k_{\varepsilon\alpha}$, $K_{\alpha\varepsilon}$, $k_{\alpha\varepsilon}$, whereas the stiffness coefficients of sub-matrix IV K_α, k_α are located between the ones from the plain and the ones for the non-symmetrically profiled seal. Regarding the damping coefficients, the use of symmetrically profiled seals reduced the direct damping coefficients of the first sub-matrix, i.e. C, significantly.

In conclusion, it can be stated that the use of profiled seal geometries both affect the static and dynamic characteristics of the annulus. Regarding the dynamic force and moment characteristics, it becomes clear that not only the well-researched force characteristic is mainly influenced by the profiling, but also the much less well-researched tilt and moment characteristics. This leads to a need for further investigation, focusing especially on the additional rotordynamic coefficients.

ACKNOWLEDGEMENTS

The financial support of the Federal Ministry for Economic Affairs and Energy (BMWi) due to an enactment of the German Bundestag under Grant No. 03EE5036B and KSB SE & Co. KGaA as well as the financial support of the industrial collective research programme (IGF no. 21029 N/1), supported by the

Federal Ministry for Economic Affairs and Energy (BMWi) through the AiF (German Federation of Industrial Research Associations e.V.) due to an enactment of the German Bundestag is gratefully acknowledged. Furthermore we acknowledge support by the Deutsche Forschungsgemeinschaft (DFG – German Research Foundation) and the Open Access Publishing Fund of Technical University of Darmstadt. Special gratitude is also expressed to Mr. Christian Thielen for the careful conduction of the experiments.

REFERENCES

[1] M.M.G. Kuhr, G. Ludwig, and P.F. Pelz, "Measurement and simulation of the dynamic characteristics of plain and profiled annular seals," *IOP Conference Series: Earth and Environmental Science*, vol. 774, no. 1, p. 012073, 2021, doi: 10.1088/1755-1315/774/1/012073.

[2] A.C. Hagg, "The influence of oil-film journal bearings on the stability of rotating machines," *J. Appl. Mech.*, vol. 13, no. 3, pp. A211–A220, 1946, doi: 10.1115/1.4009564.

[3] A.C. Hagg and G.O. Sankey, "Some dynamic properties of oil-film journal bearings with reference to the unbalance vibration of rotors," *J. Appl. Mech.*, vol. 23, no. 2, pp. 302–306, 1956, doi: 10.1115/1.4011305.

[4] D.W. Childs, "The space shuttle main engine high-pressure fuel turbopump rotordynamic instability problem," *J. Eng. Power*, vol. 100, no. 1, pp. 48–57, 1978, doi: 10.1115/1.3446326.

[5] D.W. Childs, C.C. Nelson, T. Noyes, and J.B. Dressman, "A high-Reynolds-number seal test facility: Facility description and preliminary test data," *NASA. Lewis Research Center Rotordyn. Instability Probl. in High-Performance Turbomachinery*, 1982. [Online]. Available: https://ntrs.nasa.gov/citations/19830007370

[6] S.R. Lang, *Effiziente Berechnung von Gleitlagern und Dichtspalten in Turbomaschinen*, ser. Forschungsberichte zur Fluidsystemtechnik. Aachen: Shaker Verlag, 2018, vol. Band 18.

[7] M.M.G. Kuhr, *Dynamische Eigenschaften axial durchströmter Ringspalte*, 1st ed., ser. Forschungsberichte zur Fluidsystemtechnik. Düren: Shaker Verlag, 2022, vol. Band 29, doi: 10.2370/9783844086102.

[8] M.M.G. Kuhr, R. Nordmann, and P.F. Pelz, "Dynamic force and moment characteristics of annular gaps - simulation results and evaluation of the relevance of the tilt and moment coefficients," *J. Tribol.*, vol. 145, no. 1, p. 011801, 2022, doi: 10.1115/1.4055180.

[9] M.M.G. Kuhr, "Identification of the dynamic force and moment characteristics of annular gaps using linear independent rotor whirling motions," *Mech. Syst. Signal Proc.*, vol. 187, p. 109936, 2023, doi: 10.1016/j.ymssp.2022.109936.

[10] M.M.G. Kuhr, S.R. Lang, and P.F. Pelz, "Static force characteristic of annular gaps – experimental and simulation results," *J. Tribol.*, vol. 144, no. 11, p. 111804, 2022, doi: 10.1115/1.4054792.

[11] D.W. Childs, *Turbomachinery rotordynamics: Phenomena, modeling, and analysis*, ser. A Wiley Interscience publication. New York: Wiley, 1993.

[12] F. Simon and J. Frêne, "Analysis for incompressible flow in annular pressure seals," *J. Tribol.*, vol. 114, no. 3, pp. 431–438, 1992, doi: 10.1115/1.2920902.

[13] F. Simon and J. Frêne, "Rotordynamic coefficients for turbulent annular misaligned seals," *Rotating machinery - Dynamics; Proceedings of the 3rd International Symposium on Transport Phenomena and Dynamics of Rotating Machinery (ISROMAC-3)*, pp. 207–222, 1992.

[14] L. San Andrés, "Effect of shaft misalignment on the dynamic force response of annular pressure seals," *Tribol. Trans.*, vol. 36, no. 2, pp. 173–182, 1993, doi: 10.1080/10402009308983146.

[15] L. San Andrés, "The effect of journal misalignment on the operation of a turbulent flow hydrostatic bearing," *J. Tribol.*, vol. 115, no. 3, pp. 355–363, 1993, doi: 10.1115/1.2921643.

[16] L. San Andrés, Z. Yang, and D.W. Childs, "Thermal effects in cryogenic liquid annular seals—part ii: Numerical solution and results," *J. Tribol.*, vol. 115, no. 2, pp. 277–284, 1993, doi: 10.1115/1.2921002.

[17] E. Storteig, "Dynamic characteristics and leakage performance of liquid annular seals in centrifugal pumps," Ph.D. dissertation, Norwegian University of Science and Technology, NTNU, Trondheim, 1999.

[18] N. Gibbons, C. Watson-Kassa, C. Goyne, and M. He, "Circumferentially grooved seal flow field analysis based on effective film thickness to improve bulk flow models," *J. Eng. Gas. Turbines Power*, vol. 144, no. 11, p. 111021, 2022, doi: 10.1115/1.4055412.

[19] N. Gibbons and C. Goyne, "Form shear stress (fss) correction in bulk flow analysis of grooved seals based on effective film thickness," *J. Tribol.*, vol. 146, no. 1, p. 014401, 2023, doi: 10.1115/1.4063190.

[20] Y. Kanemori and T. Iwatsubo, "Experimental study of dynamic fluid forces and moments for a long annular seal," *J. Tribol.*, vol. 114, no. 4, pp. 773–778, 1992, doi: 10.1115/1.2920947.

[21] Y. Kanemori and T. Iwatsubo, "Forces and moments due to combined motion of conical and cylindrical whirls for a long seal," *J. Tribol.*, vol. 116, no. 3, pp. 489–498, 1994, doi: 10.1115/1.2928871.

[22] T. Neumer, *Entwicklung einer Versuchsanlage mit aktiver Magnetlagerung zur Parameteridentifikation von Fluid-Struktur-Interaktionen in Strömungsmaschinen: Zugl.: Kaiserslautern, Univ., Diss*, ser. Fortschritt-Berichte VDI Reihe 11, Schwingungstechnik. Düsseldorf: VDI-Verl., 1994, vol. 203.

[23] M. Matros, A. Ziegler, and R. Nordmann, "Fluid structure interactions in annular seals of centrifugal pumps," *Tribol. Trans.*, vol. 38, no. 2, pp. 353–363, 1995, doi: 10.1080/10402009508983415.

[24] D.W. Childs and K. Hale, "A test apparatus and facility to identify the rotordynamic coefficients of high-speed hydrostatic bearings," *J. Tribol.*, vol. 116, no. 2, pp. 337–343, 1994, doi: 10.1115/1.2927226.

[25] J. Alex Moreland, D.W. Childs, and J.T. Bullock, "Measured static and rotordynamic characteristics of a smooth-stator/grooved-rotor liquid annular seal," *J. Fluids Eng.*, vol. 140, no. 10, p. 101109, 2018, doi: 10.1115/1.4040762.